Light Metals 2011 *Edited by: Stephen J. Lindsay*
TMS (The Minerals, Metals & Materials Society), 2011

NEW APPARATUS FOR CHARACTERIZING ELECTRICAL CONTACT RESISTANCE AND THERMAL CONTACT CONDUCTANCE

Nedeltcho Kandev[1], Hugues Fortin[1], Sylvain Chénard[1], Guillaume Gauvin[2], Marie-Hélène Martin[2] and Mario Fafard[2]

[1] Institut de Recherche d'Hydro-Québec (IREQ), 600 avenue de la Montagne, Shawinigan (Québec), Canada, G9N 7N5
[2] NSERC/Alcoa Industrial Research Chair MACE[3] and Aluminium Research Centre-REGAL, Laval University, Sciences and Engineering Faculty, Adrien-Pouliot Building, Quebec City (Québec), Canada, G1V 0A6

Keywords: Aluminium reduction cell, anode connection, anode stub contact, anode power losses, electrical contact resistance, thermal contact conductance

Abstract

A new apparatus for characterizing electrical contact resistance and thermal contact conductance has been developed and tested. The heating of the samples inside the apparatus was achieved via induction heating of a stainless steel billet to create a powerful heat generator instead of the commonly used convection furnace. With this equipment, the thermo-electro-mechanical (TEM) behavior of metal-carbon and metal-metal interfaces can be reproduced using a controlled inert gas environment, temperature up to 1000°C and mechanical pressure up to 2 MPa. A major advantage of this new concept is that the temperature equilibrium of the samples can be reached quickly (within two or three hours) while precisely controlling the heat flux. Recent experimental results performed on steel-carbon samples show that this concept is feasible and very efficient. This apparatus will be used to establish the constitutive laws of interfaces for electrical contact resistance and thermal contact conductance in the electrode connections to support numerical modeling of the aluminium reduction cell.

Introduction

Theoretical and experimental investigation of the thermo-electro-mechanical (TEM) behavior of the stub-anode connection is not an easy task, as it involves complex interactions between non-linear thermal, electrical, mechanical and surface phenomena. Nevertheless, computer modelling is exceptionally useful for understanding these complex phenomena and optimizing the anode design and the fabrication process. However, to build a representative numerical model of the aluminium reduction cell, it is important to correctly predict the thermal contact conductance and the electrical contact resistance (ECR) as a function of both pressure and temperature. The development of constitutive laws based on laboratory measurements is, therefore, a crucial task.

Carbon-cast iron-steel interface phenomena are regulated by the powerful fully-coupled thermo-electro-mechanical behavior of the assembly. While increasing the temperature, the materials are expanding, creating a higher contact pressure at the interfaces and decreasing the ECR. With decreased ECR, the local Joule dissipation is lowered, affecting the thermal field and so on until the thermodynamic equilibrium is reached. This stabilization of the TEM fields can take some time.

The objective of this work is to design a new apparatus employing induction heating, rather than a conventional convection furnace, as a heat generator to achieve better control of heat flux and to reach thermal equilibrium more rapidly. With this equipment, it will be possible to identify parameters of constitutive laws for the ECR and the thermal contact conductance for metal-carbon and metal-metal interfaces for implementation into a Finite Element Method (FEM) code. These laws may lead to further promising research, investigating the effect of new cast iron recipes on the ECR as well as clad to transversal bar contact resistance or the steel-cast iron interfaces degradation that has been pointed out by Kandev and Fortin [1].

Previous work

The ECR establishes the current distribution across the different interfaces and is responsible for the high voltage losses in the anode connection. To characterize the ECR, a lab-scale reproduction of the operating condition in the cell demonstrating the thermal, electrical and mechanical fields is needed.

In 1976, Peterson [2] instrumented an anode with voltage probes and thermocouples and found that the ECR was responsible for 25% of the global voltage drop in the anode. Two years later, Peterson [3] studied the effect of changing cast iron volume in the stub hole relative to temperature distribution. In 1984, Brooks and Bullough [4] attempted to optimize cast iron thickness in the stub hole to minimize anode cracking. They found that ECR was a function of both temperature and contact pressure.

In 1992, Sørlie and Gran [5] built an apparatus to measure the ECR of steel-to-carbon interfaces. A 60-mm diameter cylindrical piece of cathode block was linked with a cylindrical layer of mild steel at each end to form a sandwich sample of two different materials. Subsequently, the sample was put in a tube furnace having a controlled environment, using nitrogen gas to avoid corrosion. The same setup was later used by Hiltmann et al. [6] for the measurements of the cathode cast iron interfaces. From these experiments, unfortunately, no constitutive laws were developed for ECR that could be used in a FEM code.

By 2000, Richard et al. [7, 8] had reproduced the Sørlie and Gran [5] experiment at room temperature, using anode carbon

material. With a calibration based on experimental data from Sørlie and Gran [5], they were able to develop a constitutive law for ECR as a function of both temperature and pressure in a form of the Weibull law. Richard et al. [7, 8] incorporated this law into an FEM code and built a pie-shaped 3D model of a stub hole to study the impact of new flute design on the voltage drop.

In 2003, Laberge et al. [9] built a new test bench to characterize the thermo-electrical properties of the anode-coke bed-cathode interfaces during the preheating of the cell. Based on the same principle as the Sørlie and Gran [5] experiment, the sample was placed under a controlled environment with argon gas and resistant insulating material was placed around the sample to avoid corrosion of the carbon material. By changing the temperature and the mechanical pressure, they were able to characterize the thermal contact conductance and the electrical contact resistance of the anode-bed coke-cathode interfaces which are critical for modeling the electrical preheating of cells.

In 2009, Richard et al. [10] published the parameter values of the constitutive law at operating temperature which had been developed back in 2001. Using this constitutive law, recent publications [10, 11, 12] have since demonstrated that with FEM software, it is now possible to construct a coupled thermo-electro-mechanical (TEM) model of a full 3D anode. Such models are very useful for experimenting with new designs and will help the aluminium industry to achieve its energy efficiency objectives.

Basic concept

A new test bench was designed, constructed and tested, using induction heating of a stainless steel billet as a thermal generator to heat the sample. By precisely controlling the power injected in the sample, thermal equilibrium of the heat flux can be achieved very rapidly within two or three hours. A simplified schema of the concept design of the apparatus is shown in Figure 1.

The stainless steel billet is heated by induction using cylindrical copper coil wrapped around the billet. To prevent overheating of the copper coil at high induction heating power, the coil is water-cooled.

The heat flux is transferred from the billet to the carbon-cast-iron-steel "sandwich" samples using a metal disk with good thermal and electrical conductivity (Ni for example). The disk is added to ensure that the thermal and the electrical flux lines will be perpendicular to the surface.

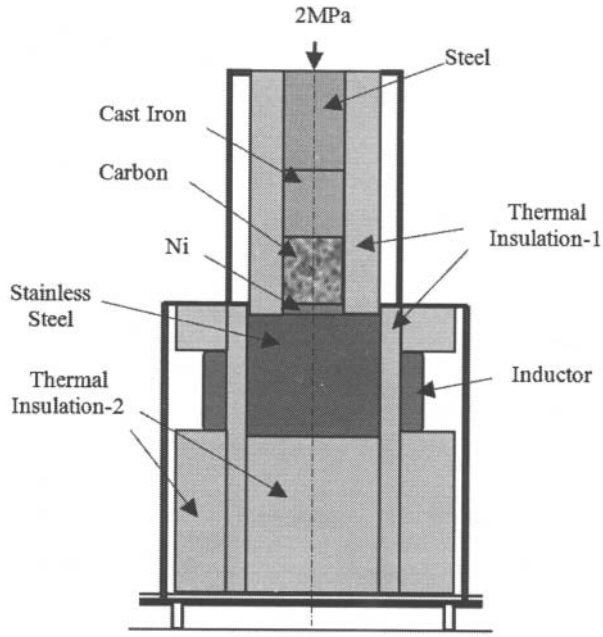

Figure 1: Simplified schema of the concept design

To minimize the heat losses, a high-quality thermal insulation (thermal insulation 1) is wrapped around the sample and around the stainless steel billet to limit the outgoing radial heat flux. Also, several layers of a special thermal insulation (thermal insulation 2) resistant to high mechanical pressure and high temperature are placed under the billet for thermal insulation and mechanical support.

TEM behavior of the interfaces inside the apparatus can be reproduced using temperatures ranging from 20°C up to 1000°C and mechanical pressure up to 2 MPa. In addition, a DC current is applied between the stainless steel billet and the top of the samples, representing the same current density that is applied at the contact surfaces in an actual operating cell. Also, to limit the air oxidation of the billet and the samples during the experiments at high temperature, a controlled inert gas environment is anticipated.

Numerical modelling

To validate this new concept, a transient thermo-electromagnetic 2D axisymmetric model was built using the computer package COMSOL Multiphysics 3.4. This model is based on the geometry of the apparatus shown in Figure 1. The physical model chosen to solve this problem is the coupling of electromagnetic induction current model with the classical heat transfer by conduction model. The problem is considered as symmetrical and the thermal and electrical characteristics of the involved materials (steel, carbon, cast-iron and thermal insulations) are considered homogenous and temperature-dependent. To simplify the numerical solution, all interfaces between materials are considered ideal. Finally, the geometry of the coil is represented by a slab of copper having an equivalent current.

The electromagnetic domain is delimited by an air cylinder. On the external boundaries of this air domain the magnetic and

electric conditions are fixed to: $\vec{n} \times \vec{A} = 0$ and $\vec{n}.\vec{J} = 0$, where $\vec{n}$ is normal vector to the boundary, A is the magnetic vector potential and J is the current density vector. The interior boundaries conditions assume continuity of the medium, corresponding to a homogenous Neumann condition.

The thermal domain is also delimited by the air cylinder with 20°C imposed temperature on the external boundaries. A temperature of 23°C is imposed in the copper stub representing the "water cooled" induction coil. To simplify the numerical solution, neither the thermal radiation nor the heat losses between interfaces are considered here.

The problem is solved using a time-dependent solver and convergence is achieved when the residual value of the equations are below 1e-6.

Several induction heating cases were simulated at different power supplies and frequencies to validate the concept and to optimize the system design. An example of temperature distribution solution at 7000 seconds time step is shown in Figure 2 for an induction heating power of 4050 W operating at a frequency of 2800 Hz. The results demonstrate that with such an induction heating generator, the temperature in the upper portion of the sample can reach 500°C very quickly.

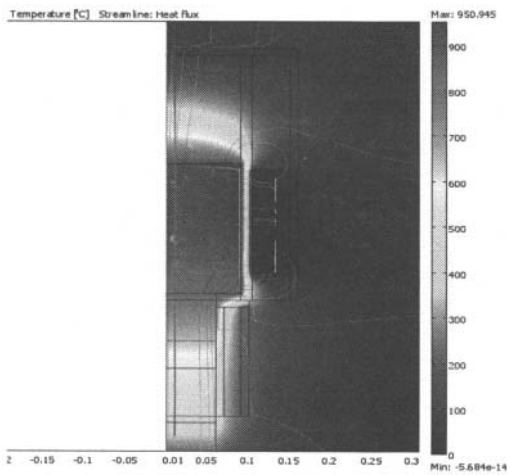

Figure 2: Temperature distribution in the model at 4050 W induction heating power and 2800Hz

Figure 3 illustrates the temperature evolution close to the axis of the system (red line in Figure 2) during induction heating up to 7000 seconds and the temperature distribution of the system at different time intervals between 3000 and 7000 seconds. It can be seen that 3000 seconds after the start of the induction heating system, the maximum temperature in the stainless steel billet reaches 435°C and at 7000 seconds of heating time, the billet reaches 925°C.

The software allows the calculation of the outgoing heat fluxes and both thermal and electrical losses in the system. For the case considered and illustrated in Figure 2 and 3, the outgoing thermal flux represents 1828 W of power. 7000 seconds after heating began the induction power was decreased to approximately 1820 W in order to compensate for the outgoing thermal flux and losses.

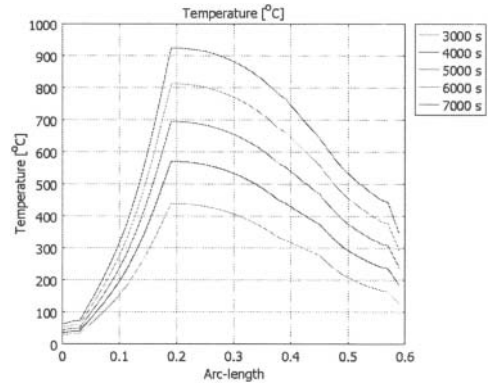

Figure 3: Temperature evolution and distribution on the cylindrical axis of the system.

To verify if thermal equilibrium could be reached, the induction heating power was set to 1820 W. Figure 4 presents the temperature evolution during induction heating between 7500 seconds and 9000 seconds at induction heating power of 1820 W, maintaining the 2800 Hz frequency. Figure 4 shows that the thermal losses are completely compensated and the system reaches thermal equilibrium very quickly at about 930°C.

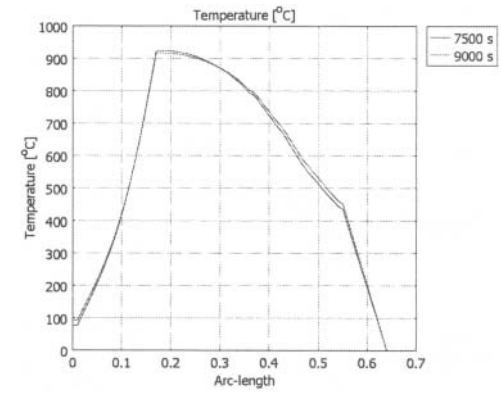

Figure 4: Temperature distribution on the cylindrical axis of the system at 1820 W and 2800 Hz

The simulation results have demonstrated that the concept of a water cooled induction coil provides a very efficient solution. At 2800 Hz, the total current in the coil is about 5800 Amps. By using a coil with 20 spires, for example, the supplying current will be:

$$I_{coil} = \frac{I_{Tot}}{n} = \frac{5800}{20} = 290 Amps \qquad (1)$$

This induction coil design was used to construct the apparatus.

Design and construction of the apparatus

The apparatus was constructed with a variety of components. For the electrical portion, a 35-kW induction generator was used, having the possibility of varying power and frequency with a capacitor bank for the frequency adaptation.

From the numerical simulation results, the inductor was designed using 20 spires of ½" diameter copper pipe. To determine the optimal frequency for the generator, the inductor characteristics were measured with an HP 4194A Impedance/Gain-Phase Analyzer. Principal characteristics are listed in Table 1, where f is the frequency, L the inductance, R the resistivity with the electrical load (stainless steel billet), R_o resistivity without the load, ***Qmeas*** the quality factor measured, ***Cres*** the capacitance at resonance frequency and finally, the ***Eff elec*** is the electrical efficiency of the induction that is calculated from the equation ***(R-Ro)/R***.

Table 1: Calculated and measured electrical characteristics of the induction coil

f	L	R	Qmeas	Ro	Cres	Eff elec
Hz	H	mOhm		mOhm	µF	%
700	4,44E-05	60,00	2,80	21,2	1165,33	64,7
800	4,37E-05	66,00	2,90	23,0	905,68	65,2
900	4,24E-05	69,70	3,00	28,0	737,20	59,8
1000	4,13E-05	76,92	3,05	30,0	613,47	61,0
2000	3,70E-05	109,00	4,00	45,0	171,15	58,7
2800	3,68E-05	126,00	5,67	48,1	87,80	61,8
3000	3,60E-05	130,00	5,68	48,7	78,18	62,5

From those results, the frequency of 2800 Hz was chosen, respecting the capacitance limitation of the generator while demonstrating good electrical efficiency.

As for mechanical loading, initially force was applied on the sample using a lever arm system having different weight at the end, as seen in Figure 5. The inductor, the different thermal insulation and the water cooling system are also shown here.

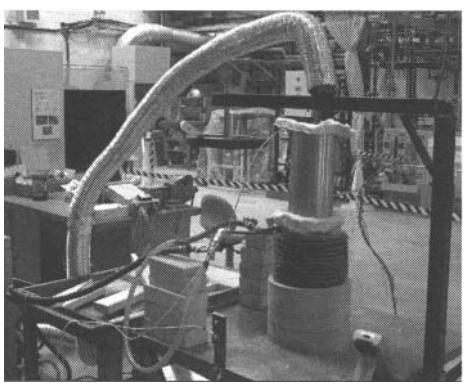

Figure 5: Apparatus in operation

In the future, the lever arm will be replaced by a manual press of 1-ton capacity which will apply a constant pressure up to 2 MPa on the sample. Also, to measure the pressure applied on the sample, a Tovey Engineering pancake type load cell will be used. In addition, all heating systems will be protected with a Nylon and G-9 shell. A stainless steel tube, with a half-open top, will contain the sample and the inert gas during the test, to avoid the oxidation of the material.

For the initial test, only the stainless steel and the carbon were used. The samples of 50.8 mm diameter and 150 mm height were placed between the nickel disk and the mechanical pressure system seen in Figure 6.

Figure 6: Sample under mechanical pressure

The temperature and the voltage drop monitoring were logged with a computer and an Agilent 34970A acquisition system. The thermocouples used were K-type and the voltage drops were measured directly from the thermocouples. The sample and the billet were instrumented with, respectively, 7 and 4 thermocouples measuring the temperature and the voltage drop. Probe arrangement in the billet (left) and in both carbon and steel (right) can be seen in Figure 7.

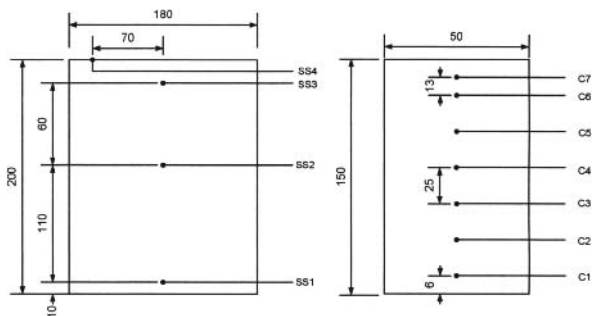

Figure 7: Probe arrangement in the stainless steel billet (SSx) and the carbon (Cx) (mm)

Experimental study

The first part of the experimental study was conducted only on the induction heating generator to verify the plausibility of the concept and the efficiency of the coupling at a frequency of 2800 Hz. Using only the lower part of the apparatus in Figure 1, i.e. without the sample and the mechanical pressure, the stainless steel billet was heated for about half an hour at a power of 10 kW. After that time, the power generator was turned off, but the data acquisition system continued to monitor the temperature for another fifty minutes. Figure 8 presents the temperature for the thermocouple in different locations on the stainless steel billet as a function of time.

The first test results showed that the electromagnetic coupling was excellent and that within half an hour, the temperature on the top of the billet could reach about 450°C. After the power generator was shut off, (B on Figure 8), the temperature slowly decreased to 400°C. It is interesting to note that two different incidents occurred during this test. At A, there was a power failure because the operating parameters of the generator were

too close to the limits. To overcome this problem, the power was decreased to obtain stability. Finally, at C, the thermal insulation on the top of the stainless steel billet was removed quickly to see the stainless steel surface at this temperature. This explains the temperature drop on the top thermocouple in the stainless steel.

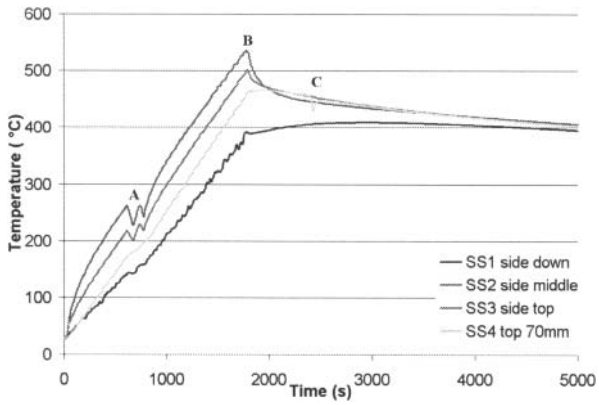

Figure 8: Temperature as a function of time in the stainless steel billet without the sample

An interesting feature of this curve is the temperature evolution in the middle section of the billet, where the induction heating is greater. Calculating the slope of about 0.3°C/s, the estimated time to reach 925°C is about fifty minutes. This result compares well with the simulation results shown in Figures 3 and 4.

A second test, employing the same operating parameters as the first test, 10 kW and 2800 Hz, was performed to validate the sample heating time and procedure. This involved mounting the carbon and steel samples on the nickel slab on the billet surface as seen in Figure 6. All the materials were instrumented, respecting the thermocouple location detailed in Figure 7. A current of 20 Amps and mechanical pressure of 0.3 MPa were applied to the sample. Figure 9 shows the temperature in the stainless steel billet as a function of time.

The billet was heated up for one hour. After a quick power adjustment (A), the sample was heated up until it reached 550°C (B). At point B, the power was decreased to achieve thermal equilibrium until the power was shut down at 700°C (C). The test shows that it is very easy to achieve temperatures up to 700°C within the hour. After the power was shut down, the temperature slowly decreased, following an exponential behavior. These results also demonstrate that the heat flux is controlled precisely, modifying the power input thus reducing the temperature in the sample rapidly. Efficiently attaining thermal equilibrium in this manner will be very useful.

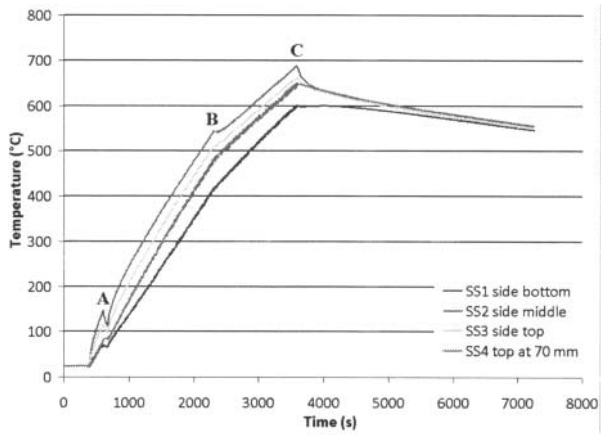

Figure 9: Temperature as a function of time in the stainless steel with the sample and the electrical current

Figure 10 portrays the temperature in the carbon sample as a function of time. The results show that within the hour, the sample temperature is over 500°C in the bottom of the sample. The temperature distribution in the carbon showed that the thermal equilibrium could not be achieved within the hour due to the thermal properties of the carbon and the carbon-steel interface behavior and the controlled argon gas environment. After the test, no trace of oxidation was observed, validating the effectiveness of the controlled argon gas environment.

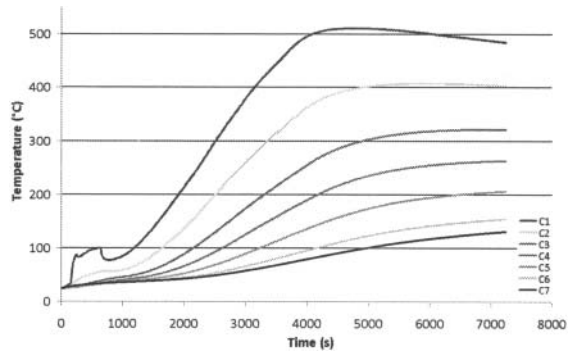

Figure 10: Temperature as a function of time in the carbon sample with current applied

In Figure 11, the temperature of all thermocouples is presented as a function of their positions, at a given time, in both carbon and steel. Results show that thermal contact conductance is weak between carbon and steel, having a drop of about 20°C at the interface (green line). Also, temperature distribution in carbon seems to follow more of a polynomial than a linear behavior as opposed to the linear behavior of the steel. For the characterization of the interfaces, a minimum gradient in the sample is required, especially in the carbon.

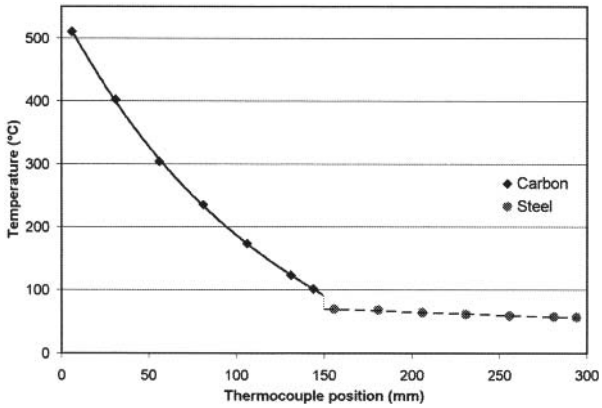

Figure 11: Temperature of the different thermocouples as a function of thermocouple position in carbon and steel at 5000s

Finally, differences between the experimental data and the numerical modelling stem from the initial condition that all interfaces between the materials are considered ideal. In the actual test, ECR and thermal contact conductance play a crucial role in electrical and thermal distribution like shown in Figure 11. Special care in the experimental setup should be given to interface cleanliness to avoid the presence of unwanted particles between the interfaces.

Conclusion

Using induction heating technology, a stainless steel billet has been designed as a powerful heat generator for heating the carbon-cast iron-steel material used in the aluminium industry. With FEM modelling, several induction heating cases were simulated to validate the concept and to optimize the design and procedure. The simulation results showed the importance of water cooling of the inductor for frequency of 2800 Hz, with a total current of 5800 Amps. The model could be reused for different applications involving induction heating technology such as the preheating of the stub before cast iron sealing.

The main advantage of this new apparatus is that temperature equilibrium of the samples can be reached very quickly (within two or three hours) while precisely controlling the heat flux. *In situ* operating conditions in the anode stub hole connection could be reproduced by putting a carbon-steel sample in the heat generator and applying mechanical pressure and electrical current on the sample. With the same TEM behavior of the materials, this new apparatus will be used initially to characterize the metal-carbon and metal-metal interfaces to determine new constitutive laws for these interfaces. These laws will be included in FEM software such as FESh^{++} to test new anode concepts or optimize the anode connection.

Finally, the versatility of this new apparatus would permit the characterization of the steel stub deterioration in the anode or in the bus bar/aluminium rod connection. It could also be very useful for the optimization of the cast iron composition for the anode or cathode connection.

Acknowledgements

The authors would like to thank Donald Picard from Laval University for support for the apparatus design, especially for the mechanical part and Claude Belzile from IREQ for the experimental test measurements.

References

1. N. Kandev and H. Fortin: Electrical losses in the stub-anode connection: Computer modeling and laboratory characterisation. In Proc. TMS Light Metals, pp. 1061-1066, 2009.
2. R.W. Peterson: Temperature and voltage measurements in Hall cell anodes. In Proc. TMS Light Metals, pp. 365-382, 1976.
3. R.W. Peterson: Studies of stub to carbon voltage. In Proc. TMS Light Metals, pp. 367-378, 1978.
4. D. G. Brooks and V. L. Bullough: Factors in the design of reduction cell anodes. In Proc. TMS Light Metals, pp. 961-976, 1984.
5. M. Sorlie and H. Gran: Cathode collector bar to carbon contact resistance. In Proc. TMS Light Metals, pp. 779-787, 1992.
6. F. Hiltmann, J. Mittag, A. Støre and H. A. Øye: Influence of temperature and contact pressure between cast iron and cathode carbon on contact resistance. In Proc. TMS Light Metals, pp. 277-283, 1996.
7. D. Richard, M. Fafard, R. Larcroix, P. Cléry and Y. Maltais.: Aluminum reduction cell anode stub hole design using weakly coupled thermo-electro-mechanical finite element models. Finite elements in analysis and design 37, pp. 287 - 304, 2001.
8. D. Richard, M. Fafard, R. Larcroix, P. Cléry and Y. Maltais: Carbon to cast iron electrical contact resistance constitutive model for finite element analysis. Journal of Materials Processing technology 132, pp. 119-131, 2003.
9. C. Laberge, L. Kiss and M. Desilets: The influence of the thermo-electrical characteristics of the coke bed on the preheating of an aluminum reduction cell, In Proc. TMS Light Metals, pp. 207-211, 2004.
10. D. Richard, P. Goulet, O. Trempe, M. Dupuis and M. Fafard: Challenges in stub hole optimization of cast iron rodded anodes. In Proc. TMS Light Metals, p. 1067-1071, 2009.
11. H.Fortin, M. Fafard, N. Kandev and P. Goulet: FEM analysis of voltage drop in the anode connector assembly. In Proc. TMS Light Metals, pp. 1055-1060, 2009.
12. Marc Dupuis. Development and application of an ANYS based thermo-electro-mechanical anode stub hole design tool. In Proc. TMS Light Metals, pp.433-438, 2010